Ceramics International 45 (2019) 7458–7467

Contents lists available at ScienceDirect

Ceramics International

journal homepage: www.elsevier.com/locate/ceramint

Influence of polyol structure and molecular weight on the shape and properties of $Ni_{0.5}Co_{0.5}Fe_2O_4$ nanoparticles obtained by sol-gel synthesis

Thomas Dippong[a,*], Oana Cadar[b], Erika Andrea Levei[b], Iosif Grigore Deac[c], Firuta Goga[d], Gheorghe Borodi[e], Lucian Barbu-Tudoran[e]

[a] Technical University of Cluj-Napoca, North University Center of Baia Mare, Department of Chemistry and Biology, 76 Victoriei Street, 430122 Baia Mare, Romania
[b] INCDO-INOE 2000, Research Institute for Analytical Instrumentation, 67 Donath Street, 400293 Cluj-Napoca, Romania
[c] Babes-Bolyai University, Faculty of Physics, 1 Kogalniceanu Street, 400084 Cluj-Napoca, Romania
[d] Babes-Bolyai University, Faculty of Chemistry and Chemical Engineering, 11 Arany Janos Street, 400028 Cluj-Napoca, Romania
[e] National Institute for Research and Development of Isotopic and Molecular Technologies, 67-103 Donath Street, 400293 Cluj-Napoca, Romania

ARTICLE INFO

Keywords:
Mixed Co-Ni ferrite
Polyol
Thermal decomposition
Nanoparticles
Crystallinity degree
Magnetic properties

ABSTRACT

This paper presents the formation and decomposition of silica embedded metal carboxylates obtained using Co-, Fe- and Ni- nitrates and polyols with different structure and molecular weight (1,2-ethanediol, 1,2-propanediol, 1,3-propanediol, 1,4-butanediol, 1,2,3-propanetriol). The thermal behavior of carboxylate precursors (oxalic, malonic, lactic, hydroxymalonic and succinic) is similar for all used polyols, both the formation and decomposition of precursors occurring in two stages. However, the mass loss slightly increases with increasing of the diol chain length and significantly increases with the presence of a supplementary, nonreactive secondary hydroxyl group. X-ray diffraction shows the formation of NiO single phase or NiO and $CoFe_2O_4$ mixtures below 750 °C, and of mixed Co-Ni ferrite single phase at 1000 °C, while Fourier transformed infrared spectroscopy confirms the formation of silica matrix and the formation and decomposition of carboxylate precursors. Transmission electron microscopy shows spherical nanoparticles of different size. The $Ni_{0.5}Co_{0.5}Fe_2O_4$ nanocrystallites size (4.3–28.1 nm) and relative crystallinity (4–100 a.u.) increase with the annealing temperature, the diol chain length and the distance between hydroxyl groups. The coercive field (0.015–0.6 T) and saturation magnetization (21.5–25 emu/g) of gels annealed at 1000 °C also increase for longer chain length diols.

1. Introduction

Due to their unique structure, morphology, chemical, optical, electrical and magnetic properties and wide applications in several technological fields, $CoFe_2O_4$ or $NiFe_2O_4$ nanoparticles have attracted considerable attention [1,2]. $CoFe_2O_4$ is a well-known hard magnetic material with extraordinary magnetic property (high saturation magnetization (M_S) and coercivity (H_c)), high thermal and chemical stability that makes it suitable as recording media, refrigeration agent, sensors, antibacterial and photo-catalysts for the degradation of dyes [3–7]. $NiFe_2O_4$ is a soft magnetic material with low M_S, H_c and conductivity, good permeability, high electrochemical stability, that can be applied for magnetic cores and drug delivery, magnetic fluids, microwave absorbers, low energy inductors, medical instruments, telecommunication, photo-catalytic degradation of dyes, gas sensors and medical diagnostics [3,8–11].

By combining $CoFe_2O_4$ and $NiFe_2O_4$, superparamagnetic nanoparticles of mixed spinel ferrite such as $Ni_{0.5}Co_{0.5}Fe_2O_4$ are obtained. This mixed Co-Ni ferrites have new chemical, structural and magnetic properties, and versatile applications in communications, medicine and nanotechnology [3,5,12,13]. Co-Ni ferrites were obtained by co-precipitation, hydrothermal, sol-gel, aerosol, sonochemical, microemulsion, surfactant-assisted route, citrate precursor technique, microwave-assisted flash combustion technique, reverse and normal micelles, reflux method, high energy mechanical ball milling, thermal decomposition and auto-combustion methods [3–5,12,13]. The co-precipitation method is widely used as it allows the simple control of synthesis parameters and nucleation growth, and produces nanoparticles with homogenous particles size distribution [14,15]. The sol-gel method is used to obtain multi-component spinel oxides with homogenous composition and high purity [9]. The magnetic character of Co-Ni ferrites strongly depends on the sizes, shape, purity and magnetic stability of the component particles [8]. The ferromagnetic ferrites can become superparamagnetic due to the disorder of single

* Corresponding author.
E-mail address: dippong.thomas@yahoo.ro (T. Dippong).

https://doi.org/10.1016/j.ceramint.2019.01.037
Received 23 December 2018; Received in revised form 5 January 2019; Accepted 5 January 2019
Available online 07 January 2019

magnetic domain particles with smaller size than the critical size, when thermal fluctuation drastically reduces M_S and H_c [8,9].

Our previous studies indicated that longer chain precursors embedded in silica matrix favor the formation of single phase $CoFe_2O_4$ at lower temperatures [15]. Regarding the magnetic properties, H_c of nanocomposites increases with the diol chain length, while M_S is higher in case of 1,2-ethanediol (1.2-ED) and 1,4-butanediol (1.4-BD) use as diol source, than in case of 1.2-propanediol (1.2-PD) and 1,3-propanediol (1.3-PD) [16].

This paper aims to study the effect of number and position of hydroxyl functional groups in polyol on the formation of Fe-, Co- and Ni-carboxylate precursors and the obtaining of mixed Co-Ni ferrites ($Ni_{0.5}Co_{0.5}Fe_2O_4$). The formation and decomposition of carboxylate precursors was investigated by thermal analysis and Fourier transform infrared (FT-IR) spectroscopy. The formation of crystalline phases was studied by X-ray diffraction (XRD), while the shape, morphology, size and agglomeration degree of nanoparticles were investigated by transmission electron microscopy (TEM) and scanning electron microscopy (SEM). The variation of M_S vs. Hc of $CoFe_2O_4$ and $NiFe_2O_4$ was studied by magnetic measurements.

2. Experimental

Through the synthesis, analytical grade reagents (Merck) were used without any further purification. Co-Ni ferrite ($Ni_{0.5}Co_{0.5}Fe_2O_4$) embedded in a silica matrix was obtained by a modified sol-gel method using $Fe(NO_3)_3{\cdot}9H_2O$, $Co(NO_3)_3{\cdot}6H_2O$, $Ni(NO_3)_2{\cdot}6H_2O$ in 4:1.1 M ratio and nitrate to polyol (1.2-ED, 1.2-PD, 1.3-PD, 1,2,3-propanetriol (1.2.3-PT) and 1.4-BD) to tetraethylorthosilicate (TEOS) molar ratio of 1:1:1. The synthesis was conducted at room temperature, in aqueous ethanol solution. HNO_3 was added to adjust the acidity. The resulted clear solution was stirred for 30 min and kept at room temperature until gelation. The NCF-1.2ED, NCF-1.2PD, NCF-1.3PD, NCF-1.2.3PT, NCF-1.4BD gels were grinded and dried at 40 °C (4 h) and 180 °C (4 h), respectively. The synthesized precursors were thermally treated at 500 °C (4 h) and afterwards annealed at 800 and 1000 °C.

The formation and decomposition of carboxylate precursors were investigated by thermogravimetry (TG), derivative thermogravimetry (DTG) and differential thermal analysis (DTA) using a SDT Q600 type instrument, in air up to 1000 °C at 10 °C·min^{-1} and alumina standards. The FT-IR spectra were recorded on 1% KBr pellets using a Spectrum BX II spectrometer. The XRD patterns were recorded using a Bruker D8 Advance diffractometer with $CuK_{\alpha 1}$ radiation (λ = 1.54056 Å). The TEM observation carried out on a Hitachi HD2700 electron microscope equipped with digital image recording system and photographic film image, were used to examine the size, shape and clustering of $Ni_{0.5}Co_{0.5}Fe_2O_4$ nanoparticles, while the particle size distributions were determined using the UTHSCSA ImageTool Software. The morphology and dispersion of samples were investigated by scanning electron microscopy (SEM) using a Hitachi SU8230 microscope. The magnetic measurements were performed using a vibrating sample cryogen-free VSM magnetometer (Cryogenic Limited). The hysteresis loops were recorded in magnetic fields from −2–2 T, at room temperature. Magnetization vs. magnetic field measurements were performed to find M_S up to 5T. The samples were embedded in epoxy resin to prevent $Ni_{0.5}Co_{0.5}Fe_2O_4$ nanoparticles movement.

3. Results and discussion

The DTA and TG curves of gels dried at 40 and 180 °C reveal the thermal behavior and mass loss of gels with temperature increase (Fig. 1). In case of NCF-1.4BD dried at 40 °C, the DTA curve shows 3 processes: (i) loss of water (8.9% mass loss in TG) absorbed on the surface and in the pores of silica gel, indicated by the endothermic effect at 74 °C; (ii) formation of Fe, Co and Ni succinates by redox reaction between nitrates and polyol indicated by the endothermic effect at 145 °C attributed to break of intermolecular bonds, followed by the exothermic effect at 188 °C attributed to the oxidation of marginal –OH [14–17] (20.5% a mass loss in TG); (iii) decomposition of succinates into α-Fe_2O_3, Co_3O_4, NiO and formation of $Ni_{0.5}Co_{0.5}Fe_2O_4$ indicated by the intense exothermic (261 °C) and the small exothermic (320 °C) effects. The total mass loss on TG curve is 60.6%. In case of NCF-1.4BD dried at 180 °C, the DTA-TG curve reveals an endothermic effect at 91 °C attributed to water loss (6.5% mass loss) and an intense exothermic effect at 345 °C attributed to formation and decomposition of succinate precursors into oxides and formation of Co-Ni ferrite. The slow mass loss up to 1000 °C is attributed to polycondensation and dehydroxylation of silica matrix. The highest mass loss (69.5%) on the TG curve is observed for the decomposition of 2-hydroxy-malonate precursor in case of NCF-1.2.3PT (40 °C), probably due to the decomposition of the supplementary secondary –OH group, beside the two primary –OH, present in the other samples. The DTA curve shows an endothermic effect at 68 °C attributed to water loss, an exothermic (156 °C) and an endothermic (174 °C) effect attributed to Fe-, Co- and Ni-hydroxy malonates formation and, respectively, to vaporization of unreacted 1.2.3-PT from the matrix pores and two exothermic effects (277 and 308 °C) attributed to decomposition of the precursors into mixed Co-Ni ferrite. In case of NCF-1.2.3PT dried at 180 °C, the DTA-TG diagram reveals two overlapping exothermic effects (311 and 335 °C) attributed to decomposition of precursors, determining a mass loss of 59.3%. The formation of Co-Ni ferrite ends around 400 °C [14–17]. The thermal behavior of NCF-1.2PD and NCF-1.3PD is similar. The water loss lake place between 64-73 °C for gels dried at 40 °C and 85104 °C for gels dried at 180 °C, respectively. In case of gels dried at 40 °C, the formation and decomposition of metal-malonates (NCF-1.3PD) and metal-lactates (NCF-1.2PD) take place in two stage processes at similar temperatures. The formation of carboxylate precursors is indicated by the exothermic (140 °C) and endothermic (170 °C) effects, while their decomposition into mixed Co-Ni ferrite is shown by two exothermic effects at 274 and 347 °C (NCF-1.3PD) and at 258 and 346 °C (NCF-1.2PD). The total mass loss is 55% and 56%, respectively. In case of gels dried 180 °C, the decomposition of precursors takes place in a single stage as shown by the intense exothermic effect around 340 °C, associated by a mass loss of 29.1% (NCF-1.3PD) and 31.2% (NCF-1.2PD), respectively. The lack of effects to indicate the precursor's formation (130–200 °C) and the low mass loss suggest that at 180 °C the carboxylate precursors are already formed.

The DTA curve of NCF-1.2ED dried at 40 °C shows an endothermic effect at 82 °C attributed to the water loss (12.3% mass loss), an exothermic (144 °C) and an endothermic (168 °C) effect attributed to the oxalate precursors formation (20.5% mass loss) and two exothermic effects (255 and 338 °C), attributed to the oxalate precursor's decomposition and formation of mixed Co-Ni ferrites. The total mass loss is 56%. In case of gels dried at 180 °C, besides the small endothermic effect at 99 °C attributed to water loss, an intense exothermic effect appears at 320 °C, attributed to the overlapping of metal-oxalate precursor's decomposition into ferrites. The mass loss of the process is 22%.

Generally, the mass loss increases with increasing of the polyol molecular weight and chain length (from 1.2-ED to 1.4-BD) and the presence of a supplementary, non-reactive secondary hydroxyl group (1.2.3-PT).

Compared to our previous studies [14–17] on $CoFe_2O_4$, where the precursors were formed in single stage, the presence of Ni results in the formation of precursors in two stages. Similarly, the decomposition of the Co, Ni and Fe carboxylates takes place in two steps, in case of gels dried at 40 °C, while, in case of gels dried at 180 °C, the processes occurs at similar temperatures and overlaps.

Fig. 2 shows the FT-IR spectra of gels dried at 40 and 180 °C. In case of gels dried at 40 °C, a broad band appears at 3351–3417 cm^{-1} attributed to O–H stretching in precursors and to intermolecular hydrogen bonds [5]. The intense band around 1384 cm^{-1} is characteristic to asymmetric vibration of N-O bond in nitrates. This band disappear at

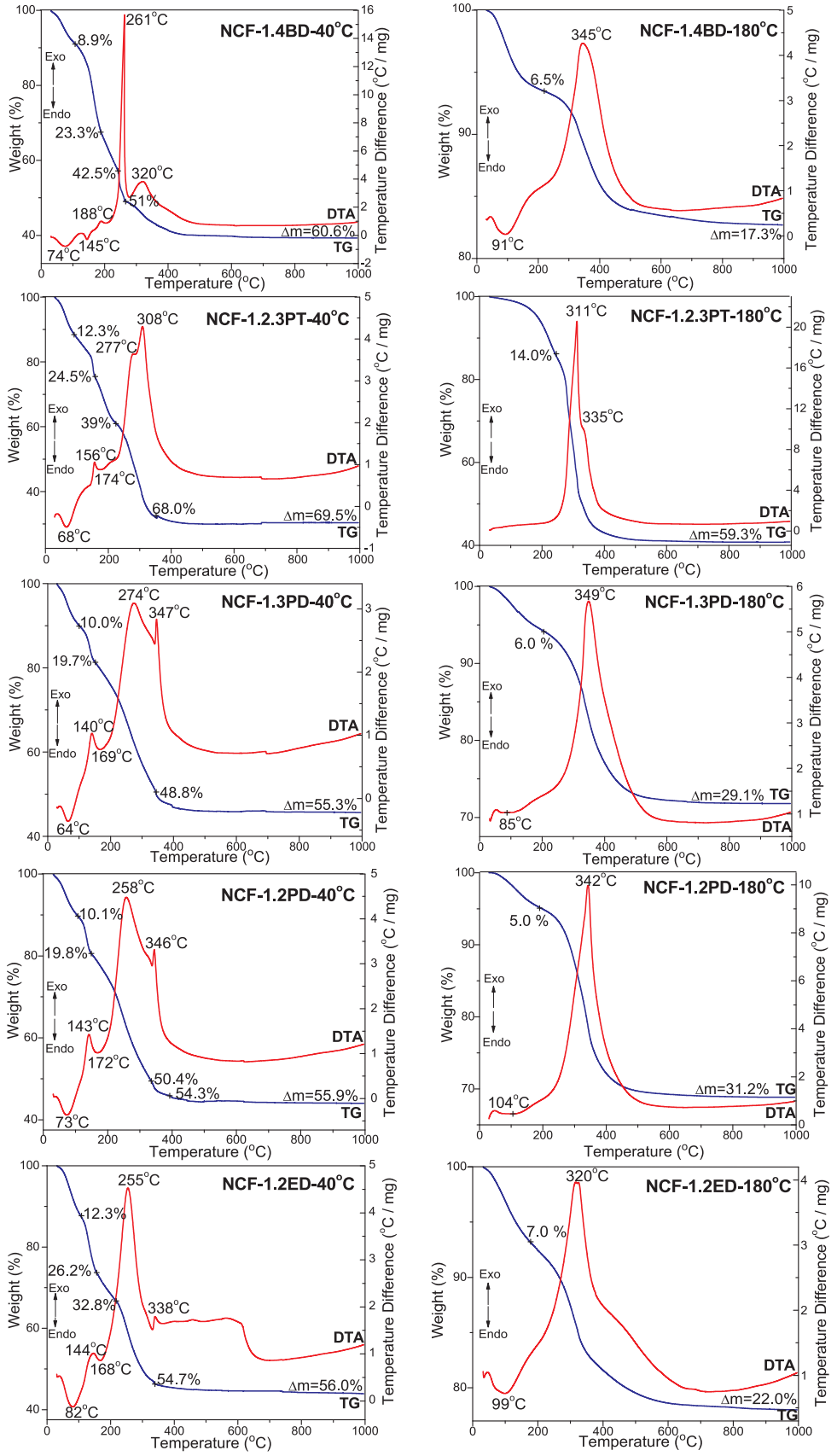

Fig. 1. TG-DTA diagrams for NCF-1.2ED, NCF-1.2PD, NCF-1.3PD, NCF-1.2.3PT, NCF-1.4BD gels at 40 and 180 °C.

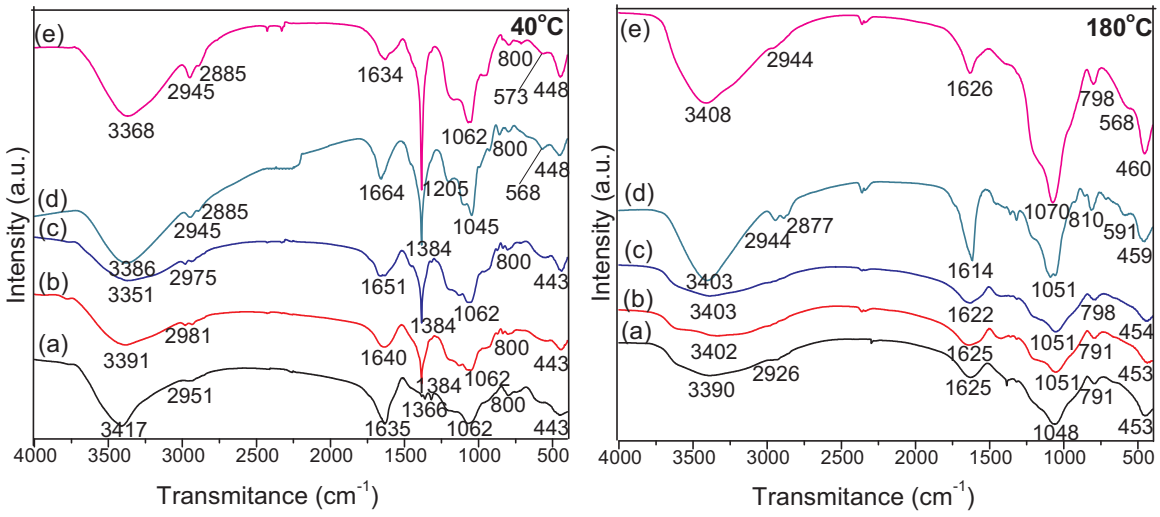

Fig. 2. FT-IR spectra of NCF-1.2ED (a), NCF-1.2PD (b), NCF-1.3PD (c), NCF-1.2.3PT (d), NCF-1.4BD (e) gels dried at 40 and 180 °C.

180 °C, suggesting that the reaction between nitrates and polyols with formation of metal-carboxylate precursors take place below 180 °C and the whole amount of nitrates are consumed up to 180 °C [14–18]. The band around 2950 cm^{-1} is characteristic to the C-H bond vibration in the methylene groups from polyols and carboxylates precursors and disappears at higher temperatures, when the precursors decompose into ferrite [14]. The intense band at 1634–1664 cm^{-1} in the spectra of gels dried at 40 °C is attributed to the overlapping of the C-O and H-O deformation vibrations [15,17]. In case of gels dried at 180 °C, the band shifts toward 1614–1626 cm^{-1} and is attributed to the C=O bond vibration in the carboxylate precursors [5,14–17]. The bands at 1045–1062 cm^{-1} (40 °C) and 1048–1070 cm^{-1} (180 °C) are attributed to the stretching vibration of C-O and Si-O-Si [14,15], while the band around 800 cm^{-1} is attributed to the symmetric stretching and band vibration of Si-O-Si chains indicating a low degree of polycondensation of the silica network [14–18]. The vibration of M-O bonds in tetrahedral sites and Si-O bonds in silica matrix are indicated by the band around 570 cm^{-1}, while the bands at 443–448 cm^{-1} (40 °C) and 453–460 cm^{-1} (180 °C) are attributed to M-O bonds vibration in octahedral sites [14,15,19].

The FT-IR spectra and the XRD patterns of gels annealed at 500, 750 and 1000 °C are presented in Fig. 3. The FT-IR spectra, at all temperatures, shows the characteristic bands for the silica matrix: O-H bond vibration in the Si-OH group (3412–3455 cm^{-1}), bending vibration of H-O-H bond (1627–1643 cm^{-1}), stretching vibration of Si-O-Si bonds (1072–1098 cm^{-1}), symmetric stretching and bending vibration of Si-O chains in the SiO_4 tetrahedron (791–809 cm^{-1}), vibration of Si-O bond (454–467 cm^{-1}) and vibration of Si-O-Si cyclic structures (568–606 cm^{-1}) [15–19]. The bands at 454–467 cm^{-1} and 568–606 cm^{-1} can be attributed also to the stretching vibration of M_{octa}-O and M_{tetra}-O bonds, respectively, from the mixed Co-Ni ferrite structure. Generally, Ni^{2+} occupies the octahedral sites, while the Co^{2+} and Fe^{3+} occupy both octahedral and tetrahedral sites [20]. The slight shift of the absorption bands towards 600 °C is a consequence of Ni presence, especially as NiO.

The XRD patterns of NCF-1.2ED, NCF-1.2PD, NCF-1.3PD gels at 500 °C show NiO unique phase (JCPDS card 47-1049), while NCF-1.2.3PT, NCF-1.4BD gels at 500 °C display a mixture of poorly crystallized $CoFe_2O_4$ (JCPDS card 22-1086) and NiO (JCPDS card 47-1049) [21]. Our previous studies indicated no formation of $CoFe_2O_4$ at 500 °C [14–17]. The gels obtained using short chain diols containing neighboring hydroxyl groups (1.2-ED and 1.2-PD) support the formation of NiO at lower temperatures (500 °C), while the gels obtained using polyols with multiple or distal hydroxyl groups favors the formation of $CoFe_2O_4$. The formation of NiO could also be the result of oxygen that can lead to the formation of intermediate products instead of ferrites or to the breaking of surface oxygen bonds that cause incomplete exchange connections [8]. At 750 °C, for all gels, the intense diffraction lines at 2θ = 37.0, 43.0 and 62.6° indicate the formation of NiO crystalline phase beside poorly crystallized $CoFe_2O_4$ (peaks corresponding to diffraction planes (111), (220), (311), (222), (400), (422), (511) and (440) confirm the formation of cubic spinel structure belonging to the space group *Fd*3*m*).

At 1000 °C, $N_{i0.5}Co_{0.5}Fe_2O_4$ with similar structure to $CoFe_2O_4$ and $NiFe_2O_4$ (JCPDS card 89–4927) is formed; the diffraction lines of $CoFe_2O_4$ are very close/overlap to those of $NiFe_2O_4$ (isostructural compounds). For NCF-1.2ED, NCF-1.2PD, NCF-1.3PD and NCF-1.2.3PT gels, a crystalline phase with lattice parameters closer to $CoFe_2O_4$, while for NCF-1.4BD, a crystalline phase with lattice parameters closer to $NiFe_2O_4$ were formed. A possible explanation for the formation of crystalline $CoFe_2O_4$ instead of $NiFe_2O_4$ is the low oxidation capacity, melting points, coefficient of thermal expansion and high electronegativity and specific heat of Ni [22].

The narrow, well-defined peaks attributed to $Ni_{0.5}Co_{0.5}Fe_2O_4$ without any secondary phase or impurity indicates the complete synthesis of pure, well-crystallized spinel ferrite [3].

The crystallites size and crystallinity can be controlled by the number and position of hydroxyl groups in polyol, the hydroxyl groups determining the saturation level at the nucleation-growth process and crystallization. The increase of nucleation process at higher temperatures (1000 °C) cause smaller and more stable particles [3].

The average crystallites size was calculated using the Scherrer equation [17].

$$D_{hkl} = \frac{0.9\,\lambda}{\beta \cos\theta} \quad (1)$$

where D is crystallites size, β is the broadening of full width at half the maximum intensity (FWHM) in radian, θ is the Bragg angle, λ is the X-ray wavelength.

The average size of nanocrystallites estimated by Scherrer equation, relative crystallinity and average particles size according to TEM are presented in Table 1. As even in the samples with the highest crystallinity (gels annealed at 1000 °C) amorphous phases are still observed, the crystallinity was expressed in arbitrary units (a.u.) instead of percentages. The degree of crystallinity is given by the ratio of crystalline diffraction area to the total diffraction area (sum of diffraction peaks and diffraction halo). The diffraction areas and diffraction halos are approximately a constant for a particular material with the same kind of scattering atoms. Considering a 100% crystallinity for the sample with

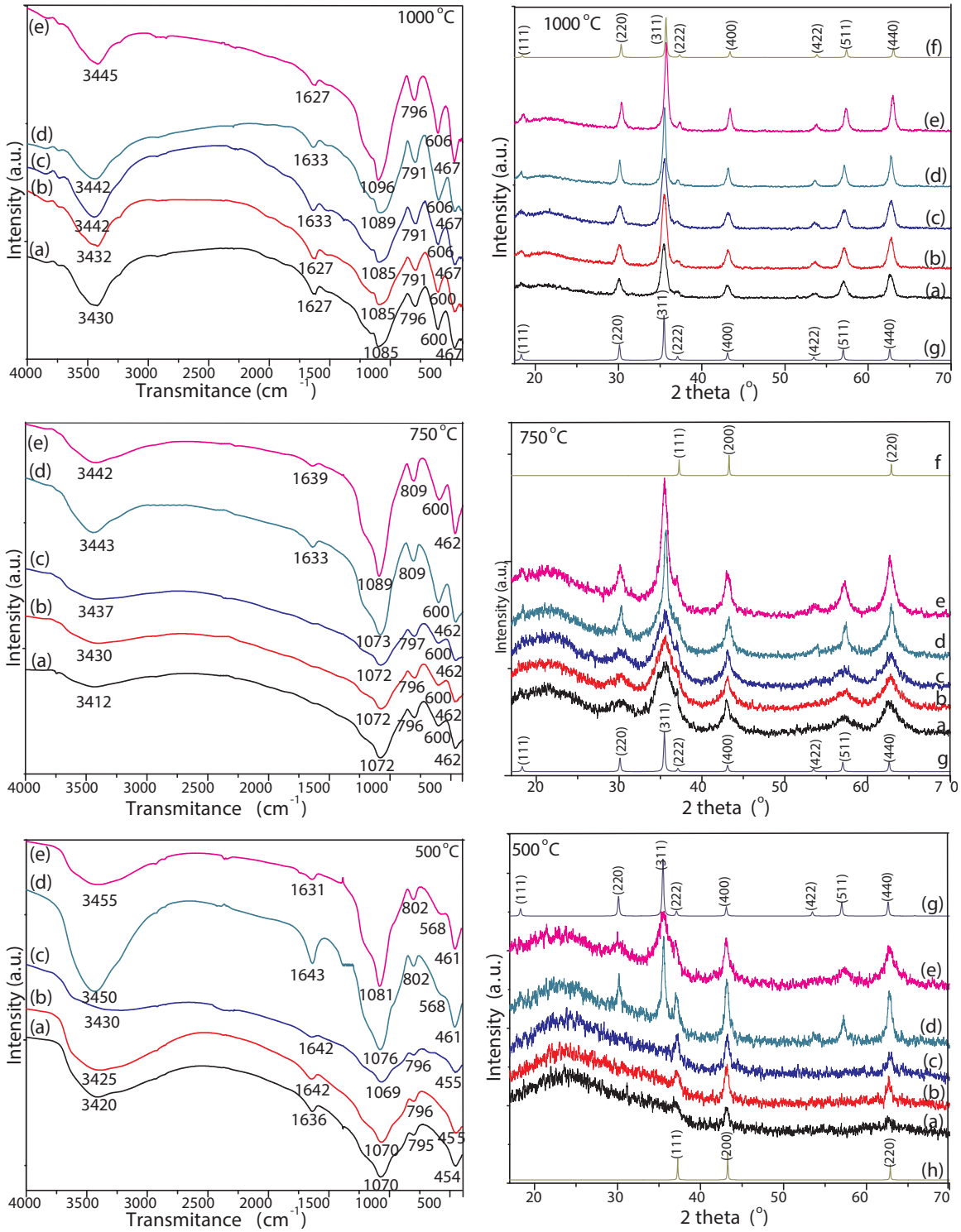

Fig. 3. FT-IR spectra and XRD patterns of NCF-1.2ED (a), NCF-1.2PD (b), NCF-1.3PD (c), NCF-1.2.3PT (d), NCF-1.4BD (e) gels annealed at 500, 750 and 1000 °C and XRD patterns of $NiFe_2O_4$ - JCPDS card 89-4927 (f), $CoFe_2O_4$, JCPDS card 22–1086 (g), NiO - JCPDS card 47-1049 (h).

the highest crystallinity (NCF-1.4BD), the crystallinity of the other gels was expressed as % form the highest crystallinity in a.u. As expected, the relative crystallinity and average particle sizes are very dependent on the preparation route [23,24]. The nanocrystallites size and crystallinity increase with the annealing temperature, the diol chain length and the distance between hydroxyl groups. Some possible explanations could be: (i) at higher temperatures, the particles connect to each-other and form larger particles, (ii) the increase of Ostwald ripper process with temperature (dissolving small crystals and redepositing onto larger crystals) and (iii) the increase of thermal energy attributed to acceleration of atomic diffusion [3]. The thermal treatment at 1000 °C leads to larger ferrite nanoparticles with good dielectric and microwave absorption properties.

The TEM images of NCF-1.2ED, NCF-1.2PD, NCF-1.3PD gels at 500, 750 and 1000 °C (Fig. 4) reveal irregularly distributed spherical shape ferrite nanoparticles. The agglomeration of nanoparticles occurs due to interactions of magnetic nanoparticles. Furthermore, the small particles have higher surface tension than the larger one, resulting in a driving

Table 1
Average size of nanocrystallites, relative crystallinity and average particles size of NCs.

Gels	Crystallite size [nm]			Relative crystallinity [a.u.]			Particle size [nm]		
	500 °C	750 °C	1000 °C	500 °C	750 °C	1000 °C	500 °C	750 °C	1000 °C
NCF-1.2ED	4.3	6.0	13.3	4.4	58.8	72.5	–	8.0	14.1
NCF-1.2PD	5.0	11.5	13.7	11.3	59.1	91.6	–	12.0	16.4
NCF-1.3PD	5.1	12.3	14.2	14.7	62.4	86.9	5.3	12.8	20.0
NCF-1.2.3PT	6.8	15.7	23.5	31.5	68.3	95.0	7.2	16.5	26.7
NCF-1.4BD	9.5	20.3	28.1	34.4	71.9	100	–	8.0	14.1

force that increases agglomeration [18]. The presence of Ni results in the formation of soft agglomerations consisting of particles with irregular morphology [25]. Similar to XRD, the increase of particles size with number and distance between hydroxyl groups was observed. The increase of particles size can be attributed to the growth rate of crystals following the volume expansion and supersaturation reduction of the system at high annealing temperatures [14]. Agglomeration of ferrite particles in conglomerates at 500 °C, small spherical nanoparticles at 700 °C, while at 1000 °C, well-delimited spherical particles were observed. The nanoparticle sizes increase at higher annealing temperatures, due to the low crystallinity degree at 500 and 750 °C and to the presence of NiO beside $CoFe_2O_4$. At low temperatures, due to the high nucleation rate, small and well-distributed particles were observed, while at higher temperatures, the coalescence determines the growth of particles [8].

Fig. 5 shows the elements distribution maps, EDX (energy dispersive X-ray) spectra and SEM images of gels annealed at 1000 °C. According to the distribution maps, the elements are uniformly distributed in the sample and the resulted structure is a nanocomposite with the magnetic phase dispersed in silica matrix. EDX and elements distribution analysis confirms the presence of Co, Ni, Fe, O and Si. Furthermore, the EDX analysis reveals $Ni_{0.5}Co_{0.5}Fe_2O_4/SiO_2$ agglomerated irregular shape particles that increase with the increasing number of hydroxyl groups and distance between them.

Fig. 6 shows the magnetic hysteresis loops (VSM), magnetization derivatives ($dM/d(\mu_0H)$), saturation magnetization (M_S) and coercive field (H_C) values of the $Ni_{0.5}Co_{0.5}Fe_2O_4/SiO_2$ annealed at 1000 °C. The hysteresis loops show relatively small H_c and M_S values. H_c increases with the distance between the hydroxyl groups of polyol, due to the larger magneto crystalline anisotropy of $NiFe_2O_4$, enhancing the energy of the domain wall [9]. H_c may be also increased by the spin disorder at the particle surface which can enhance exchange anisotropy due to the presence of various magnetic phases as a result of chemical disorder and broken chemical bonds [26,27]. The H_c of a magnetic material is roughly a measure of its magnetocrystalline anisotropy [20] and in our case it increases with the increase of crystallite size. This happens due to the enhancement of magneto-crystalline energy on the surface of $Ni_{0.5}Co_{0.5}Fe_2O_4$ nanoparticles, by the increase of surface area and crystallite size. The low H_c values of small size crystallites can be related to the presence of single domain particles. The preparation route can make one of the ferrites ($CoFe_2O_4$ and $NiFe_2O_4$) dominant. The orbital contribution of Co^{2+} to the magnetic moment is very significant, spin – orbit interaction is enhanced and this result in larger induced anisotropy. M_S of $Ni_{0.5}Co_{0.5}Fe_2O_4$ nanoparticles is affected by crystallinity and crystallites size with ferromagnetic behavior [3]. The use of 1.2-ED results in a H_c of 0.015T, while in the case of 1.4 BD, the H_c is 0.06T. M_S increases with the distance between hydroxyl groups, but decreases at higher number of hydroxyl groups (21.5 emu/g for 1.2-ED and 25 emu/g for 1.3-PD). Our previous work [25] proved that M_S decreases with increasing content of Ni in $Ni_xCo_{1-x}Fe_2O_4$ and in the case of our samples we can suppose that higher Ni content in the samples determine lower M_S. The particle sizes also affect the magnitude of M_S. In larger size particles, the sizes of the magnetic domains and the number of magnetic moments with parallel alignment with the magnetic field, increase giving rise to a higher M_S [16].

The preparation route induces antisite defects when a fraction of Co/Ni ions can occupy Fe sublattice sites and conversely resulting in modifications of exchange interactions between tetrahedral and octahedral sub-lattices. This fact also contributes to M_S value, crystallinity and particle size distribution [27]. The hysteresis loops are well centered, indicating the absence of ferromagnetic/antiferromagnetic interfaces [28].

The hydroxyl group influences the morphological characteristics of the magnetic powders synthesized by sol-gel method. NCF-1.4BD and NCF-1.2.3PT exhibit good ferromagnetic properties, due to their large H_c and M_S, while the other ferrites from the series show a paramagnetic behavior.

The magnetization derivative ($dM/d(\mu_0H)$) vs. applied magnetic field curves, show sharp peaks for the gels where $CoFe_2O_4$ is dominant in the mixt ferrite $Ni_{0.5}Co_{0.5}Fe_2O_4$, indicating the presence of a single magnetic phase. In the case of NCF-1.4BD dominated by $NiFe_2O_4$, in the mixt ferrite $Ni_{0.5}Co_{0.5}Fe_2O_4$, it can be seen a depreciation of magnetic phase purity, suggested by the broadening and semi-splitting trend of the peak. The broadening of the hysteresis loop can also be observed by lowering M_S and increasing H_C.

4. Conclusions

The paramagnetic spinel ferrite $Ni_{0.5}Co_{0.5}Fe_2O_4$ was obtained using a polyol based sol-gel method. The formation of Fe-, Co- and Ni- carboxylate precursors takes place in two stages, more or less evidenced on the DTA. At 1000 °C, the XRD and FT-IR studies confirmed the formation of single phase spinel structure with high purity and crystallinity. For NCF-1.2ED, NCF-1.2PD, NCF-1.3PD and NCF-1.2.3PT a crystalline phase with lattice parameters closer to $CoFe_2O_4$, while for NCF-1.4BD gel, a crystalline phase with lattice parameters closer to $NiFe_2O_4$ were formed. At 500 °C, for all gels and at 750 °C, for gels obtained using short chain diols, a single NiO phase was observed. The crystallites size and crystallinity can be controlled by the number and position of hydroxyl groups in polyol, the hydroxyl groups determining the saturation level at the nucleation-growth process and crystallization. The TEM images confirmed the increase of particle sizes from 5.3 to 37.5 nm with increasing annealing temperature, diol chain length and distance between hydroxyl groups. The SEM micrographs revealed largely agglomerated, well-defined nanoparticles with broad particle size distribution. M_S increased with the distance between hydroxyl groups, but decreased for higher number of hydroxyl groups in the polyol. The best magnetocrystalline anisotropy was determined for ferrites obtained from 1.4-BD, which exhibits the highest H_c, due the exchange anisotropy and to spin disorder at the particles' surface. The high H_c and M_S and consequently the high physical stability, make $Ni_{0.5}Co_{0.5}Fe_2O_4/SiO_2$ suitable to be used in preparation of high-density magnetic recording disk.

Acknowledgments

This work was supported by: (i) Ministry of Economy, Romania, Sectorial Operational Program "Increase of Economic Competitiveness"

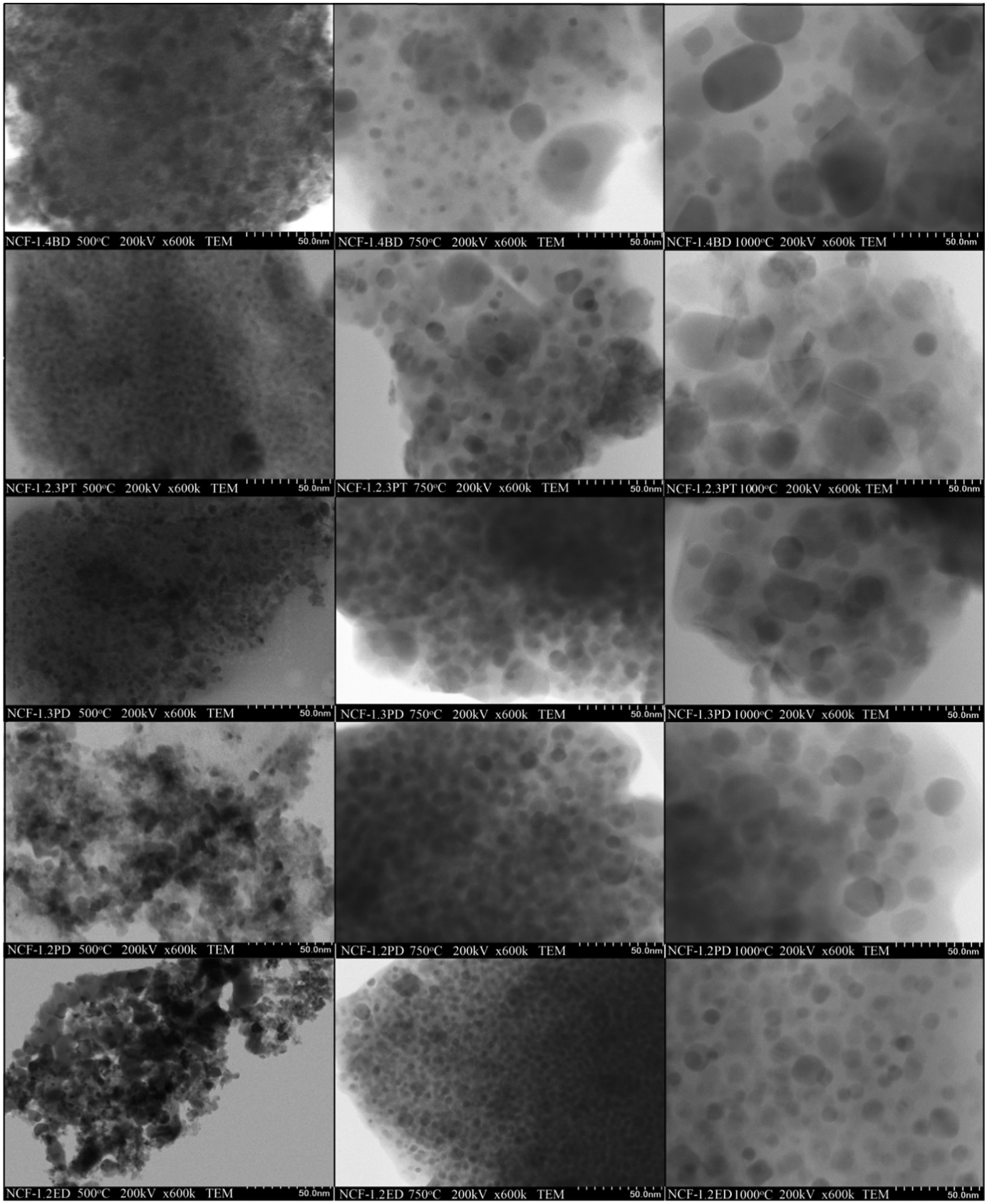

Fig. 4. TEM images of NCF-1.2ED, NCF-1.2PD, NCF-1.3PD, NCF-1.2.3PT, NCF-1.4BD gels annealed at 500, 750 and 1000 °C.

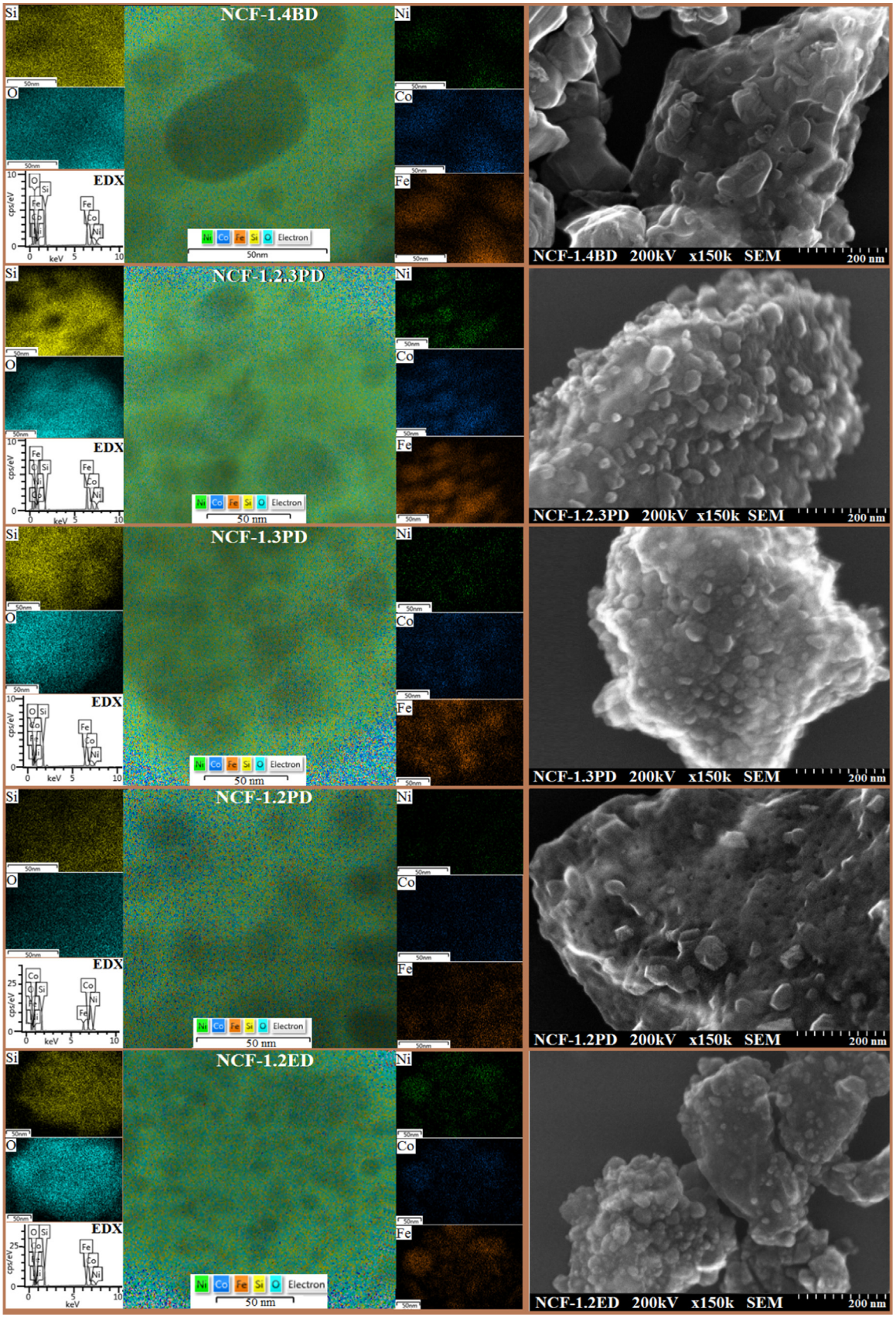

Fig. 5. Elements distribution maps, EDX spectra and SEM images of NCF-1.2ED, NCF-1.2PD, NCF-1.3PD, NCF-1.2.3PT, NCF-1.4BD gels annealed at 1000 °C.

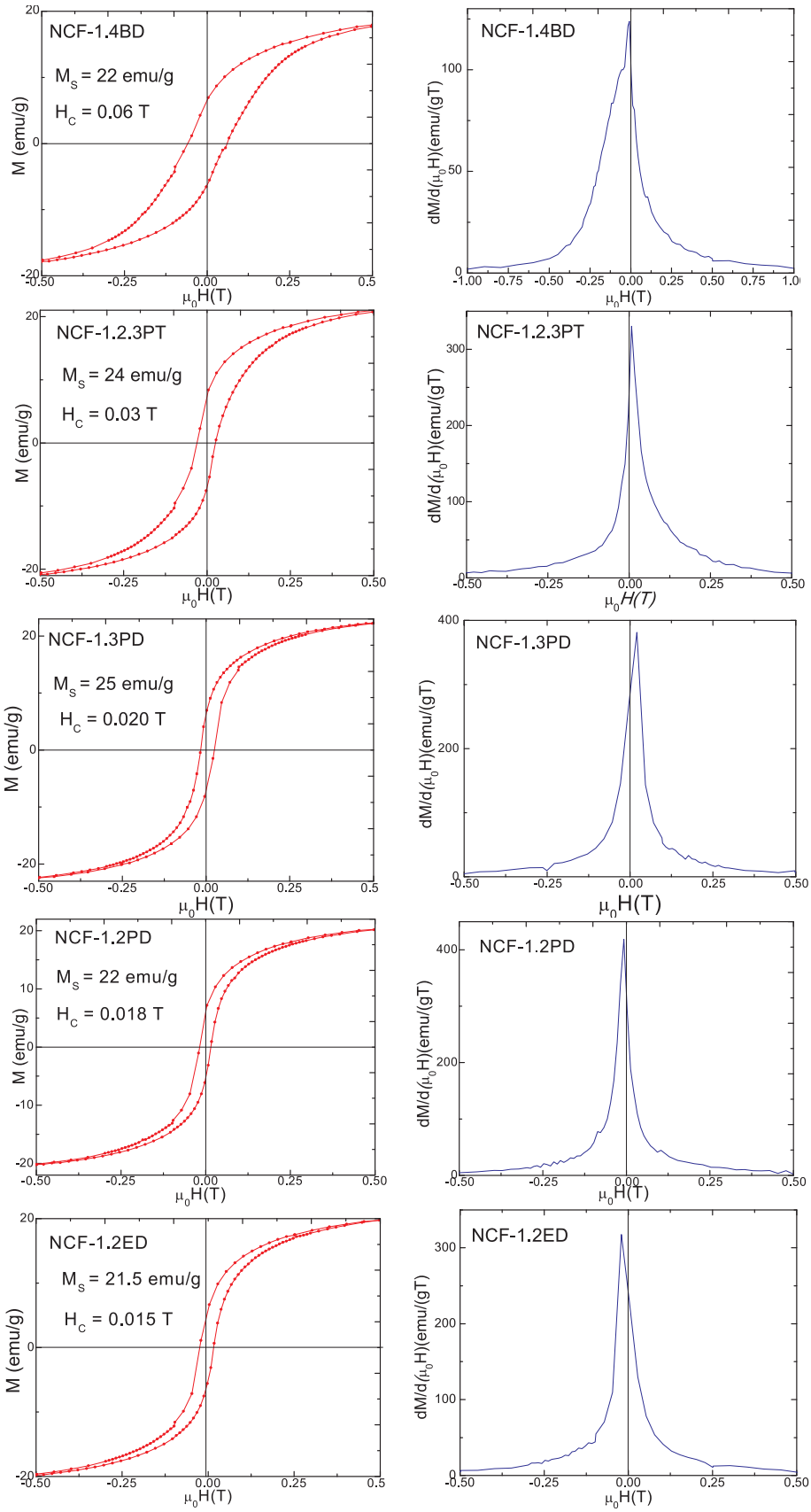

Fig. 6. Magnetic hysteresis loop and magnetization derivative of NCF-1.2ED, NCF-1.2PD, NCF-1.3PD, NCF-1.2.3PT, NCF-1.4BD gels annealed at 1000 °C.

Priority Axis II, Grant Number 1887, INOVA-OPTIMA, code SMIS-CSNR 49164, (ii) Ministry of Research and Innovation, CNCS - UEFISCDI, Romania grant number: PN-III-P4-ID-PCE-2016-0534, PN-III-P4-ID-PCCF-2016-0112 and PN-III-P1-1.1-MC-2018-0816.

References

[1] M.M.L. Sonia, S. Anand, S. Blessi, S. Pauline, A. Manikandan, Effect of surfactants (PVB/EDTA/CTAB) assisted sol-gel synthesis on structural, magnetic and dielectric properties of $NiFe_2O_4$ nanoparticles, Ceram. Int. 44 (2018) 22068–22079.

[2] S. Asiri, M. Sertkol, H. Gungunes, Md Amir, A. Manikandan, I. Ercan, A. Baykal, The temperature effect on magnetic properties of $NiFe_2O_4$ nanoparticles, Inorg. Organomet. Polym. Mater. 28 (2018) 1587–1597.

[3] A.K. Agustina, J. Utomo, E. Suharyadi, T. Kato, S. Iwata, Effect of synthesis parameters on crystals structures and magnetic properties of cobalt nickel ferrite nanoparticles, IOP Conf. Ser. Mater. Sci. Eng. 367 (2018) 012006.

[4] M.R. de Freitas M, G.L. Gouveia, L.J. Dalla Costa, A.J.A. de Oliveira, R.H.G.A. Kiminami, Microwave assisted combustion synthesis and characterization of nanocrystalline nickel-doped cobalt ferrites, Mater. Res. -Ibero-Am. J. 19 (2016) 27–32.

[5] S. Torkian, A. Ghasemi, R.S. Razavi, Cation distribution and magnetic analysis of wideband microwave absorptive $Co_xNi_{1-x}Fe_2O_4$ ferrites, Ceram. Int. 43 (2017) 6987–6995.

[6] A. Manikandan, R. Sridhar, S. Arul Antony, S. Ramakrishna, A simple Aloe vera plant-extracted microwave and conventional combustion synthesis: morphological, optical, magnetic and catalytic properties of $CoFe_2O_4$ nanostructures, J. Mol. Struct. 1075 (2018) 188–200.

[7] A. Manikandan, M. Durka, S. Arul Antony, A novel synthesis, structural, morphological, and opto-magnetic characterizations of magnetically separable spinel $Co_xMn_{1-x}Fe_2O_4$ ($0 \le x \le 1$) nano-catalysts, J. Supercond. Nov. Magn. 27 (2014) 2841–2857.

[8] K. Maaz, G.-H. Kim, Single domain limit for $Ni_xCo_{1-x}Fe_2O_4$ ($0 \le x \le 1$) nanoparticles synthesized by coprecipitation route, Mater. Chem. Phys. 137 (2012) 359–364.

[9] T. Shanmugavel, S. Gokul Raj, G. Rajarajan, G. Ramesh Kumar, Tailoring the structural and magnetic properties and of nickel ferrite by auto combustion method, Proc. Mat. Sci. 6 (2014) 1725–1730.

[10] G. Mathubala, A. Manikandan, S. Arul Antony, P. Ramar, Photocatalytic degradation of methylene blue dye and magneto-optical studies of magnetically recyclable spinel $Ni_xMn_{1-x}Fe_2O_4$ ($x = 0.0$–1.0) nanoparticles, J. Mol. Struct. 113 (2016) 79–87.

[11] A. Manikandan, S. Arul Antony, S. Sridhar, S. Ramakrishna, M. Bououdina, A simple combustion synthesis and optical studies of magnetic $Zn_{1-x}Ni_xFe_2O_4$ nanostructures for photoelectrochemical applications, J. Nanosci. Nanotechnol. 15 (2015) 4948–4960.

[12] S. Phumying, S. Labuayai, E. Swatsitang, V. Amornkitbamrung, S. Maensiri, Nanocrystalline spinel ferrite (MFe_2O_4, M = Ni, Co, Mn, Mg, Zn) powders prepared by a simple Aloe vera plant-extracted solution hydrothermal route, Mater. Res. Bull. 48 (2013) 2060–2065.

[13] A. Baykal, N. Kasapoglu, Z. Durmus, H. Kavas, M.S. Toprak, Y. Koseoglu, CTAB-assisted hydrothermal synthesis and magnetic characterization of $Ni_xCo_{1-x}Fe_2O_4$ nanoparticles (x = 0.0, 0.6, 1.0), Turk. J. Chem. 33 (2009) 33–45.

[14] T. Dippong, E.A. Levei, O. Cadar, F. Goga, L. Barbu-Tudoran, G. Borodi, Size and shape-controlled synthesis and characterization of $CoFe_2O_4$ nanoparticles embedded in a PVA-SiO_2 hybrid matrix, J. Anal. Appl. Pyrolysis 128 (2017) 121–130.

[15] T. Dippong, E.A. Levei, O. Cadar, Preparation of $CoFe_2O_4/SiO_2$ nanocomposites at low temperatures using short chain diols, J. Chem. (2017) 7943164.

[16] T. Dippong, O. Cadar, E.A. Levei, I.G. Deac, L. Diamandescu, L. Barbu-Tudoran, Influence of cobalt ferrite content on the structure and magnetic properties of $(CoFe_2O_4)_X$ $(SiO_2\text{-}PVA)_{100\text{-}X}$ nanocomposites, Ceram. Int. 44 (2018) 7891–7901.

[17] T. Dippong, E.A. Levei, O. Cadar, A. Mesaros, G. Borodi, Sol-gel synthesis of $CoFe_2O_4$:sio_2 nanocomposites - insights into the thermal decomposition process of precursors, J. Anal. Appl. Pyrolysis 125 (2017) 159–177.

[18] M.A. Ati, Z. Othaman, A. Samavati, Influence of cobalt on structural and magnetic properties of nickel ferrite nanoparticles, J. Mol. Struct. 1052 (2013) 177–182.

[19] R. Sen, P. Jain, R. Patidar, S. Srivastava, R.S. Rana, N. Gupta, Synthesis and characterization of nickel ferrite ($NiFe_2O_4$) nanoparticles prepared by sol- gel method, Mater. Today-Proc. 2 (2015) 3750–3757.

[20] A. Baykal, N. Kasapoglu, Y. Koseoglu, A.C. Basaran, H. Kavas, M.S. Toprak, Microwave-induced combustion synthesis and characterization of $Ni_xCo_{1-x}Fe_2O_4$ nanocrystals (x = 0.0, 0.4, 0.6, 0.8, 1.0), Cent. Eur. J. Chem. 61 (2008) 125–130.

[21] Joint Committee on Powder diffraction Standards- International Center for Diffraction Data, 1999.

[22] U.B. Sontu, N.G. Rao, F.C. Chou, M.V.R. Reddy, Temperature dependent and applied field strength dependent magnetic study of cobalt nickel ferrite nano particles: synthesized by an environmentally benign method, J. Magn. Magn. Mater. 452 (2018) 398–406.

[23] A. Silambarasu, A. Manikandan, K. Balakrishnan, Room-temperature superparamagnetism and enhanced photocatalytic activity of magnetically reusable spinel $ZnFe_2O_4$ nanocatalysts, J. Supercond. Nov. Magn. 30 (2017) 2631–2640.

[24] A. Manikandan, E. Hema, M. Durka, K. Seevakan, T. Alagesan, S. Arul Antony, Room temperature ferromagnetism of magnetically recyclable photocatalyst of $Cu1_{-x}Mn_xFe_2O_4\text{-}TiO_2$ ($0.0 \le x \le 0.5$) nanocomposites, J. Supercond. Nov. Magn. 28 (2015) 1783–1789.

[25] M.R. de Freitas, G.L. de Gouveia, L.J. Dalla Costa, A.J.A. de Oliveira, R.H.G.A. Kiminami, Microwave assisted combustion synthesis and characterization of nanocrystalline nickel-doped cobalt ferrites, Mater. Res. 19 (2016) 27–32.

[26] V.K. Chakradhary, A. Ansari, J.M. Akhtar, Design, synthesis, and testing of high coercivity cobalt doped nickel ferrite nanoparticles for magnetic applications, J. Magn. Magn. Mater. 469 (2019) 674–680.

[27] M.A. Ati, H. Khudhair, S. Dabagh, R.M. Rosnan, A.A. Ati, Synthesis and characterization of cobalt doped nickel - ferrites nanocrystalline by co-precipitation method, Int. J. Sci. Eng. Res. 5 (2014) 927–930.

[28] L. Rednic, I.G. Deac, E. Dorolti, M. Coldea, V. Rednic, M. Neumann, Magnetic cluster developement in $In_{1-x}Mn_xSb$ semiconductor alloys, Cent. Eur. J. Phys. 8 (2010) 620–627.